

## Experimental determination of transverse dispersivity in a helix and a cochlea

Ioannis D. Benekos,<sup>1,2</sup> Olaf A. Cirpka,<sup>3</sup> and Peter K. Kitanidis<sup>1</sup>

Received 4 November 2005; revised 27 March 2006; accepted 6 April 2006; published 12 July 2006.

[1] In porous media, transverse dispersion plays a decisive role in the dilution of conservative solutes, the decay of concentration fluctuations, and the mixing of reactive solutes. One possible approach for measuring the transverse dispersivity of homogeneous isotropic porous media is based on the principle of Taylor-Aris dispersion, where the longitudinal macrodispersion coefficient is inversely proportional to the pore-scale transverse dispersion coefficient. Taylor-Aris dispersion requires a shear flow situation. To achieve the latter in porous media, we use a helix, as previously proposed, and also a cochlea, which is spiral-shaped cavity resembling the interior a nautilus shell. We obtain experimental breakthrough curves from conservative tracer experiments and compare them to results of numerical simulation. By fitting the model we obtain the values of transverse dispersivity in various tracer tests. In our experiments we investigate porous media with relatively uniform particle distributions. Estimates of the transverse dispersivity are obtained for each experiment, and the relative advantages of each device are discussed. The two devices yield similar results. The estimated ratio of transverse dispersivity to longitudinal dispersivity agrees with the higher ratios reported in the literature.

**Citation:** Benekos, I. D., O. A. Cirpka, and P. K. Kitanidis (2006), Experimental determination of transverse dispersivity in a helix and a cochlea, *Water Resour. Res.*, 42, W07406, doi:10.1029/2005WR004712.

### 1. Introduction

[2] The importance of local transverse dispersion is now widely recognized. Kapoor and Gelhar [1994], Kitanidis [1994], Kapoor and Kitanidis [1998], and Fiori and Dagan [2000] identified local transverse dispersion as a key factor in the smoothing of concentration fluctuations and controlling the rate of dilution of conservative solutes. In heterogeneous media, local transverse dispersion transfers longitudinal spreading of solute plumes to effective mixing [Dentz *et al.*, 2000; Cirpka and Kitanidis, 2000], which is particularly important for transport of compounds that react upon mixing [Kapoor *et al.*, 1997; Oya and Valocchi, 1998; Cirpka, 2002]. Linear stochastic theory states that in steady state flows the asymptotic macroscopic transverse dispersivity is only slightly larger than the local value [Gelhar and Axness, 1983]. This is of particular relevance for plumes of continuously emitted contaminants that react with compounds from ambient water, because these plumes are controlled by effective macroscopic transverse dispersion [Cirpka *et al.*, 1999; Huang *et al.*, 2003]. For equilibrium reactions and instantaneous irreversible reactions, it can be shown that the length of such plumes is inversely proportional to the transverse dispersivity [Ham *et al.*, 2004; Liedl

*et al.*, 2005; Cirpka *et al.*, 2006]. Transverse dispersion also controls the dissolution of NAPL pools [Eberhardt and Grathwohl, 2002; Chu *et al.*, 2005] and the mass transfer of volatile compounds through the capillary fringe [Klenk and Grathwohl, 2002].

[3] Despite the importance of local transverse dispersion for reactive transport, transverse dispersivity values are rarely determined. One reason for the lack of data lies in the experimental difficulties associated with such determinations. In this paper, we start with a brief review of existing methods for the measurement of transverse dispersion. Then, we revisit the principle of Taylor-Aris dispersion in shear flow, where the longitudinal macrodispersion coefficient is inversely proportional to the local transverse dispersion coefficient. Cirpka and Kitanidis [2001] proposed to induce shear flow in a helical device. The flow velocity near the outer circumference is smaller than near the inner one resulting in a stretched breakthrough curve of a tracer injected in a pulse. They presented approximate analytical expressions for angular macrodispersion as a function of transverse dispersion. In this study, we implement the experimental setup of Cirpka and Kitanidis [2001] but use numerical modeling to simulate the results without relying on simplifying assumptions made in the latter study. Additionally, we propose an alternative device with a similar objective, the cochlea. After describing our devices and procedures, we present and discuss the results of some experiments.

### 2. Existing Experimental Methods to Determine Transverse Dispersivities

[4] Various experimental setups have been proposed and tested for determining transverse dispersion coefficients of

<sup>1</sup>Department of Civil and Environmental Engineering, Stanford University, Stanford, California, USA.

<sup>2</sup>Now at ENVIRON International Corporation, Emeryville, California, USA.

<sup>3</sup>Swiss Federal Institute of Aquatic Science and Technology, Dübendorf, Switzerland.

porous media at laboratory and field scales. One category of setups relies on introducing two miscible fluids into parallel layers in a uniform flow field [Grane and Gardner, 1961; Blackwell, 1962; Harleman and Rumer, 1963; Hassinger and van Rosenberg, 1968; Nishigaki et al., 1996]. Then, transverse dispersion coefficients are determined either by fitting transverse concentration profiles in steady state or by analyzing the solute flux passing the supposed dividing streamline at the outflow of the experimental device.

[5] Transverse dispersion coefficients have been evaluated from transient transport in parallel flow [Zou and Parr, 1993, 1994], and in interwell tracer tests [Chen et al., 1999]. Robbins [1989] used a point source in saturated laboratory column experiments and determined transverse dispersion coefficients from the decrease of concentration along the assumed centerline of the plume. Wang et al. [1987] proposed a linear graphical method for the estimation of dispersivities in which they compared the derivatives of the experimental breakthrough curve at an isolated nonaxial measurement point to analytical expressions obtained for instantaneous point source injection of a conservative tracer under steady state flow conditions.

[6] The downside of methods that are based on concentration measurements at isolated points and extraction wells [Robbins, 1989; Zou and Parr, 1993; Chen et al., 1999], or from the interpretation of spatially integrated concentration data [Blackwell, 1962; Hassinger and van Rosenberg, 1968], is that these methods are sensitive to small-scale heterogeneities shifting the center line of the concentration profiles. The resulting differences between the observed breakthrough curves and those from the analytical solution may introduce significant error in the evaluation of transverse dispersion coefficients. Also, some of the listed methods are invasive in the sense that inserting a measuring probe may locally disturb the flow field [Robbins, 1989], while others require very accurate measurements of the concentration [Grane and Gardner, 1961; Harleman and Rumer, 1963; Nishigaki et al., 1996].

[7] Seagren et al. [1999] and Eberhardt and Grathwohl [2002] performed experiments in which they measured net rates of DNAPL pool dissolution in order to determine transverse mixing coefficients. The analysis of these experiments requires a sharp interface between the NAPL and aqueous phases [Seagren et al., 1999], which is in disagreement with the capillary behavior of water at such interfaces.

[8] Mass flux of TCE from groundwater to the unsaturated zone as shown by Susset [1998] and vice versa by Jellali [2000] have been studied for determining transverse dispersivities. Klenk and Grathwohl [2002] performed an inverse pool experiment in a tank filled with sand in which a volatile tracer (TCE) was released into the unsaturated zone. The total mass flux of TCE in the groundwater was measured in the outflow of the domain. The measured mass flux is proportional to the transverse dispersion coefficient in the capillary fringe. In these experiments, entrapped air within the capillary fringe may act as "mixing chambers" and thus affect the estimates of the transverse dispersion coefficient.

[9] Cirpka et al. [2006] determined transverse dispersivities from the length of alkaline plumes in acidic ambient water, which they visualized by adding a pH indicator to both solutions. This method fails for porous media with

significant buffer capacity, i.e., in the presence of carbonates. Thus each method has its limitations. In what follows, we describe and present results using yet another type of method.

### 3. Shear Flow and Taylor-Aris Dispersion

[10] Consider flow in a duct where the longitudinal velocity depends on the location in the cross section. The simplest case may be given by laminar flow in a straight tube which was studied by Taylor [1953] and Aris [1956]. Here the velocity profile is parabolic:

$$u(r) = 2U \left( 1 - \frac{r^2}{R^2} \right) \quad (1)$$

in which  $u$  is the velocity in the axial direction at distance  $r$  from the center of the cross section;  $U$  is the mean velocity; and  $R$  is the inner radius of the tube. Then the flux-weighted cross-sectional mean concentration of a conservative tracer satisfies, after some relaxation time, the advection-dispersion equation with velocity  $U$  and macrodispersion coefficient  $D^*$

$$D^* = \frac{U^2 R^2}{48 D_m} + D_m \quad (2)$$

where  $D_m$  is the molecular diffusion coefficient. Typically, the first term of equation (2) is by orders of magnitude larger than the second. The macrodispersion coefficient can be determined from the spread of the breakthrough curve measured at the outflow of the tube. The inverse relation to the molecular diffusion coefficient  $D_m$  was used to determine  $D_m$  in capillary tube experiments [e.g., Bello et al., 1994]. There are two major advantages of this approach. First, the breakthrough curve in the outflow pipe is easy to measure experimentally without affecting the flow inside the pipe. Second, the spread of the breakthrough curve is large enough to be captured with accuracy. The inverse relationship between  $D_m$  and  $D^*$  makes the approach particularly accurate for small values of  $D_m$ .

[11] The principles of Taylor-Aris dispersion have been extended to a broad class of flows [Brenner and Edwards, 1993]. An example is the flow in a spiral or helical device filled with a porous media as described by Cirpka and Kitanidis [2001]. Applying a head difference between the inlet and the outlet, the resulting flow velocity decreases with increasing distance to the inner wall. In the resulting shear flow, a conservative solute undergoes Taylor-Aris (macro)dispersion. That is to say, the cross-sectional average of the concentration is well described by an advection-dispersion equation with constant coefficients, and the macrodispersion coefficient is inversely related to the local transverse dispersion coefficient [Cirpka and Kitanidis, 2001]. From the macrodispersion coefficient, which can be readily measured, one may infer the local transverse dispersion coefficient, in analogy to the method described by Bello et al. [1994].

[12] Cirpka and Kitanidis [2001] computed the flow field analytically, by making the approximation that the flow is two-dimensional. This approximation is reasonable when the pitch (i.e., the axial displacement in a single revolution

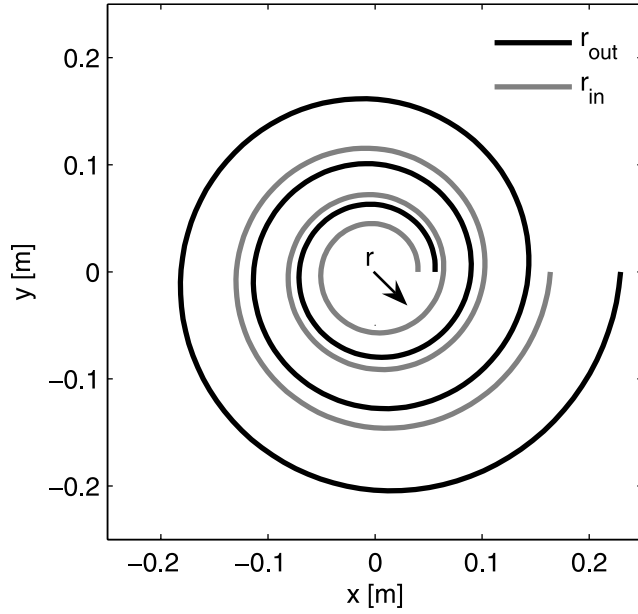


**Figure 1.** Cochlear flow channel. The gray and black lines depict the inner and outer boundaries ( $r_{in}$  and  $r_{out}$ ), respectively.

of the helix) is small compared to the dimensions of the cross section. Another, less restrictive approximation was that the traveltime in the helix is long compared to the time of mixing over the cross section. These approximations yielded closed form analytical expressions for the macrodispersion coefficient. In the present study, we employ finite element methods to produce the breakthrough curve of the mean concentration measured at the outlet while accounting for the finite length of the helix and the three-dimensionality of the flow field caused by a finite pitch.

[13] Like in the helical device, Taylor-Aris dispersion occurs in a spiral device in the form of a nautilus shell, called a cochlea. The idea underlying this device is the same as for the helical device. The shear flow enhances the spreading of the breakthrough curve of the concentration measured at the outlet. The local transverse dispersion impedes this spreading because it mixes solute between the fast inner lanes and the slower outer ones. As a consequence, the larger the transverse local dispersion, the lower the spreading that is observed at the outlet. In comparison to the helix, the cochlea can be constructed, filled and operated more easily. This method is described in section 4.

#### 4. Flow in a Cochlea

[14] A cochlea is a spiral resembling the cavity within a nautilus or snail shell, see Figure 1. Each of the boundary lines can be expressed simply in polar coordinates:

$$\frac{r}{R} = \lambda^{\frac{\theta}{2\pi}} \quad (3)$$

where  $r$  is the radial coordinate (distance from the center),  $\theta$  is the angle,  $R$  is a length scale and  $\lambda$  is a dimensionless number larger than 1 that specifies the magnification of  $r$  when  $\theta$  increases by  $2\pi$ . In other words, the line described

by equation (3) is a spiral with a radius that increases by the constant factor  $\lambda$  in every rotation. This applies also to the width of the channel and the thickness of the walls. The flow in the cochlea is two dimensional, limited to the  $\theta - r$  plane. Figure 1 shows a cochlea with 3 revolutions.

[15] The cavity can be subdivided into cells: the first cell is for  $\theta$  from 0 to  $2\pi$ , the second from  $2\pi$  to  $4\pi$ , and so on. The inner ( $r_{in}$ ) and outer ( $r_{out}$ ) boundaries of the cochlear cavity can be defined as

$$r_{in} = R\lambda^{\frac{\theta}{2\pi}} \quad (4)$$

$$r_{out} = (R - dr)\lambda^{\left(\frac{\theta}{2\pi} + 1\right)} \quad (5)$$

where  $dr$  is the initial thickness of the boundary wall that separates the cochlear cavities in each resolution. The thickness of the wall increases gradually along the conduit by a factor  $\lambda$  at each resolution. It suffices to consider flow in the first cell, because the flow net is geometrically similar in all the cells.

[16] We use complex potential theory, following the notation of *Strack* [1989]. The complex potential  $\Omega$  is defined by

$$\Omega(z) = \Phi(x, y) + i\Psi(x, y) \quad (6)$$

where  $z = x + iy = re^{i\theta}$ ;  $\Phi$  is the discharge potential; and  $\Psi$  is the stream function. One can verify that the solution to the flow problem is the superposition of two elementary solutions, a point source and a vortex, both centered at 0.

$$\Omega = -\frac{Q}{2\pi} \ln \frac{z}{R} - \frac{Q}{i \ln \lambda} \ln \left( \frac{z}{R} \right) \quad (7)$$

[17] This analytical solution has real and imaginary parts both satisfying the Laplace equation. They are:

$$\Phi = -\frac{Q}{2\pi} \ln \frac{r}{R} - \frac{Q}{\ln \lambda} \theta \quad (8)$$

$$\Psi = -\frac{Q}{2\pi} \theta + \frac{Q}{\ln \lambda} \ln \frac{r}{R} \quad (9)$$

where  $Q$  [ $L^2/T$ ] is the flow rate  $Q_{tot}$  divided by the vertical height of flow channel  $h_v$ . The constants have been set so that at  $r = R$  and  $\theta = 0$ , the potential and the stream function are 0. The complex discharge function is defined as:

$$W(z) = q_x - iq_y = -\frac{d\Omega}{dz} = \frac{Q}{2\pi} \frac{1}{z} + \frac{iQ}{\ln \lambda} \frac{1}{z} \quad (10)$$

[18] From equations (8) and (9) by considering  $\Psi = \Psi_0$  and  $\Phi = \Phi_0$  respectively we can solve for  $r$  as a function of  $\theta$  to identify streamlines and equipotentials. For a streamline,

$$r = \left( R\lambda^{\frac{\Psi_0}{Q}} \right) \lambda^{\frac{\theta}{2\pi}} \quad (11)$$

[19] Thus the streamlines are nautilus spiral lines, which verifies that the no-flux boundary conditions at the side-

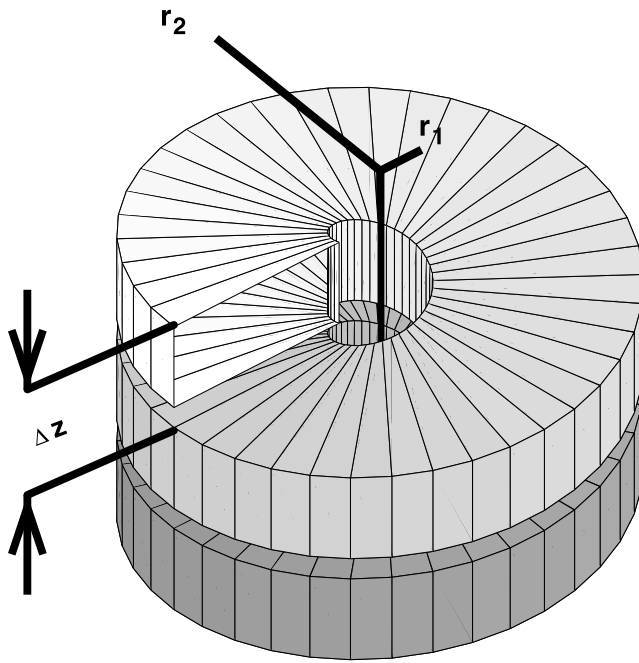


**Figure 2.** Illustration of the helical domain (here with  $n = 2.5$  revolutions), where  $r_1$  is inner radius,  $r_2$  is outer radius, and  $\Delta z$  is pitch.

walls are satisfied. From equation (8) we obtain the velocity components:

$$v_r = -\frac{1}{\eta_e} \frac{\partial \Phi}{\partial r} = \frac{Q}{2\pi r \eta_e} \quad (12)$$

$$v_\theta = -\frac{1}{\eta_e r} \frac{\partial \Phi}{\partial \theta} = \frac{Q}{r \ln \lambda \eta_e} \quad (13)$$

where  $\eta_e$  is the porosity. Thus the velocity is inversely proportional to the radial distance  $r$ .

[20] For both the helix and the cochlea, we simulate transport by applying the particle-tracking method [Prickett *et al.*, 1981], which has the advantage that it does not introduce numerical dispersion. The hydrodynamic dispersion tensor was parameterized after Scheidegger [1961].

[21] It is important that the combination of the cochlea's design parameters (number of rotations  $n$ , the initial inner radius  $r_{in}^0$ , and the ratio  $\lambda$ ) maximize the sensitivity of  $M_{2c}$ , the second central moment associated with the breakthrough curve, to the transverse dispersion parameters. For this purpose we perform particle-tracking simulations to guide our selection of the cochlea dimensions. The flow channel in the cochlea has a uniform thickness  $h_v$  equal to 0.02 m. For construction purposes, the initial thickness of the wall separating the consecutive spiral rotations  $dr$  is selected to equal 0.005 m.

[22] In the cochlea, the longitudinal dispersivity  $\alpha_\ell$  also contributes significantly to  $M_{2c}$ . The optimum design should maximize the relative contribution of  $\alpha_t$  versus  $\alpha_\ell$  to  $M_{2c}$ . We simulate different cochlea configurations and compare the relative sensitivity of  $M_{2c}$  with respect to changes in  $\alpha_t$ . Simulations with a small initial inner radius  $r_{in}^0$  and  $1.3 < \lambda$

$< 2.0$  showed greater sensitivity to changes in  $\alpha_t$ . The reason is that velocities are inversely proportional to  $r$ . When  $\lambda$  is too small, the radial velocity differences is small and so is the effect of  $\alpha_t$  on the spread of the breakthrough curve. When  $\lambda$  or  $n$  are too large, the radius  $r$  increases rapidly with  $\theta$ , the velocities decrease quickly with  $\theta$ , and molecular diffusion remains as the dominant mixing process. If the number of rotations were too small, the tracer would exit the cochlea before transverse dispersion would have a chance to decrease longitudinal macrodispersion significantly. After testing several design configurations, we have set  $r_{in}^0 = 0.04$  m and selected  $\lambda = 1.6$  and  $n = 3$ . Nonetheless, the contribution of the longitudinal dispersivity  $\alpha_\ell$  to  $M_{2c}$  is not negligible and therefore an independent estimate of  $\alpha_\ell$  is needed.

[23] To estimate the longitudinal dispersivity  $\alpha_\ell$ , we perform standard column experiments with the same porous material that is used in the cochlea. We estimate the transverse dispersion parameters by minimizing the sum of squared differences between modeled and measured concentrations in the breakthrough curve [Bates and Watts, 1988].

## 5. Experiments Using a Helix

### 5.1. Device and Procedure

[24] Two identical helical columns were manufactured at the workshop of the Institut für Wasserbau at Universität Stuttgart, Germany. All parts were made of stainless steel. The interior of each helix was made of an auger. A 1 mm deep thread with a pitch of 27 mm was cut into a solid rod with a diameter of 30 mm; 360° worm segments with an inner diameter of 28 mm, an outer diameter of 102 mm, and a flight thickness of 2 mm were screwed onto the rod and welded to the rod as well as to each other, resulting in a solid stem auger with parallel flights. Stainless steel strips, 2 mm thick and 25 mm wide, were wound and welded to the flights thus sealing the helix to the exterior. At both ends, a frame was welded to the openings in order to fix a cap with flow connectors.

[25] Each column has  $n = 60$  convolutions. The inner radius  $r_1$  is 15 mm and the outer radius  $r_2$  is 50 mm. The pitch  $\Delta z$  is 27 mm and the thickness of the flight  $\Delta z_f$  is 2 mm so that the effective thickness of the packing is 25 mm. Figure 2 illustrates the geometry of the helical domain. Both columns were filled with glass beads of uniform diameter. The dry beads were deposited into the inlet opening while the column was rotated and simultaneously vibrated. The mass of the glass beads used in the packing was measured in order to obtain a rough estimate of the porosity of the filling. To prevent gas entrapment, the dry columns were flushed with gaseous carbon dioxide prior to imbibition with degassed water. Constant discharge was guaranteed by applying a head difference between the inlet and the outlet using constant-head boxes. The tracer solutions were injected continuously into the initially tracer-free columns.

[26] Experiments with the first column were performed at Universität Stuttgart using fluorescein as tracer. Fluorescein was dissolved in deionized water at a concentration of 500  $\mu\text{g/L}$ . The pH of the tracer solution was adjusted to a value of 9 by adding sodium hydroxide, because the

**Table 1.** Flow Rates and Estimated Parameters With the Optimization Scheme for the 0.75–1.0 mm Glass Bead Tracer Experiments in the Helix<sup>a</sup>

	Experiment				Average
	1	2	3	4	
$Q_{tot}$ , m <sup>3</sup> /s	$1.50 \times 10^{-7}$	$1.00 \times 10^{-7}$	$7.50 \times 10^{-8}$	$3.83 \times 10^{-8}$	–
$\alpha_t$ , m	$5.52 \times 10^{-4}$	$3.10 \times 10^{-4}$	$3.50 \times 10^{-4}$	$3.15 \times 10^{-4}$	$3.82 \times 10^{-4}$
$\sigma_{\alpha_t}$ , m	$0.61 \times 10^{-4}$	$1.26 \times 10^{-4}$	$0.70 \times 10^{-4}$	$1.50 \times 10^{-4}$	$0.57 \times 10^{-4}$
$\eta_e$ , dimensionless	0.400	0.421	0.403	0.398	0.406

<sup>a</sup>Fluorescein tracer (grain diameter of 0.75–1.0 mm);  $\alpha_t = 1 \times 10^{-3}$  m,  $D_m = 1 \times 10^{-9}$  m, (fixed for all experiments).

fluorescence intensity of fluorescein is diminished at lower pH values. The fluorescein concentration was detected by in situ fiber-optic fluorometry [Nielsen *et al.*, 1991]. Fiber-optic probes were located in the inlet and the outlet of the helix and connected to a multichannel fluorometer, provided by Hermes Messtechnik, Stuttgart, Germany. The grain size of the glass beads used in this column ranged from 0.75 to 1 mm. Fluorometer readings were averaged over one minute and stored on a personal computer.

[27] In the second column, installed at Stanford University, two sets of experiments were performed. Glass beads ranging in diameter from 1.8 to 2.2 mm and from 0.4 to 0.6 mm were used in the first and second set of experiments, respectively. In addition to vibration and rotation, compressed air was applied periodically to achieve a more compact packing. The tracer used in these experiment is sodium bromide. The experimental setup is identical to that of the first column, except for the measuring device where an ion-selective electrode was used (model 96-35, ThermoOrion, Beverly, Massachusetts, USA). To minimize the effects of temperature fluctuations on the bromide measurements, the experiments were conducted in a temperature-regulated room. Furthermore, an automated temperature compensation probe (model 920A, ThermoOrion) was used in conjunction with the bromide electrode. The electrode is installed in a flow-through cell at the outlet of the helix. It is connected via a sensor link card to a laptop computer. A maximum injection concentration of 40 mg/L was applied in our experiments.

[28] The voltage produced by the electrode may depend on the water pressure, the flow velocity, and the grounding

setup [Lolic *et al.*, 2001]. This complicates the absolute calibration of the probe. However, since these influences did not change in the course of an experiment, the normalized concentrations (zero for no tracer, one for injection concentration) were not affected. Over a time period of several days, the electrode showed a drift. Thus the flow-through cell should be used for short-time experiments not exceeding a day in duration. For longer experiments, the fluorometer proved to be more reliable.

## 5.2. Experiments

[29] We performed four fluorescein tracer experiments at different flow rates and durations ranging from a few hours to one day (see Table 1). The measured concentrations were normalized by the inflow concentration. The flow rates in the experiments were selected so that the hydrodynamic part of the transverse dispersion  $\alpha_t|\mathbf{v}|$  is about an order of magnitude higher than the molecular diffusion coefficient  $D_m$  for minimizing the contribution of the latter in the mixing. Of course,  $\alpha_t|\mathbf{v}|$  is not known a priori but we can estimate it roughly using the porosity value obtained from the packing and assuming a value for the transverse dispersivity based on the average grain size. Two more sets of experiments (using different glass bead sizes in each set as described previously) at different flow rates are presented using the sodium bromide tracer (see Tables 2 and 3). The normalized breakthrough curves ranging from zero to one for all experiments are shown in Figure 3. Even the highest flow rate is low enough to ensure creeping flow. A direct comparison of the two tracers reveals that the breakthrough curves obtained from

**Table 2.** Flow Rates and Estimated Parameters With the Optimization Scheme for the 1.8–2.2 mm Glass Beads Tracer Experiments<sup>a</sup>

	Experiment			Average
	1	2	3	
		<i>Helix</i>		
$Q_{tot}$ , m <sup>3</sup> /s	$1.27 \times 10^{-7}$	$7.40 \times 10^{-8}$	–	–
$\alpha_t$ , m	$1.30 \times 10^{-3}$	$1.20 \times 10^{-3}$	–	$1.25 \times 10^{-3}$
$\sigma_{\alpha_t}$ , m	$0.15 \times 10^{-3}$	$0.74 \times 10^{-4}$	–	$0.05 \times 10^{-3}$
$\eta_e$ , dimensionless	0.341	0.356	–	0.349
		<i>Cochlea</i>		
$Q_{tot}$ , m <sup>3</sup> /s	$2.48 \times 10^{-7}$	$1.92 \times 10^{-7}$	$1.30 \times 10^{-7}$	–
$\alpha_t$ , m	$1.27 \times 10^{-3}$	$1.39 \times 10^{-3}$	$0.90 \times 10^{-3}$	$1.19 \times 10^{-3}$
$\sigma_{\alpha_t}$ , m	$0.21 \times 10^{-3}$	$0.20 \times 10^{-3}$	$0.15 \times 10^{-3}$	$0.15 \times 10^{-3}$
$\eta_e$ , dimensionless	0.31	0.30	0.30	0.303

<sup>a</sup>Bromide ion tracer (grain diameter of 1.8–2.2 mm);  $\alpha_t = 2.9 \times 10^{-3}$  m,  $D_m = 1 \times 10^{-9}$  m (fixed for all experiments).

**Table 3.** Flow Rates and Estimated Parameters With the Optimization Scheme for the 0.4–0.6 mm Glass Beads Tracer Experiments<sup>a</sup>

	Experiment				Average
	1	2	3	4	
	<i>Helix</i>				
$Q_{tot}$ , m <sup>3</sup> /s	$1.15 \times 10^{-7}$	$8.06 \times 10^{-8}$	$4.56 \times 10^{-8}$	–	–
$\alpha_p$ , m	$3.03 \times 10^{-4}$	$2.50 \times 10^{-4}$	$2.74 \times 10^{-4}$	–	$2.76 \times 10^{-4}$
$\sigma_{\alpha_p}$ , m	$0.61 \times 10^{-4}$	$1.26 \times 10^{-4}$	$0.70 \times 10^{-4}$	–	$0.15 \times 10^{-4}$
$\eta_{es}$ , dimensionless	0.365	0.368	0.361	–	0.365
	<i>Cochlea</i>				
$Q_{tot}$ , m <sup>3</sup> /s	$2.48 \times 10^{-7}$	$1.92 \times 10^{-7}$	$1.30 \times 10^{-7}$	$1.92 \times 10^{-7}$	–
$\alpha_p$ , m	$2.85 \times 10^{-4}$	$2.90 \times 10^{-4}$	$3.02 \times 10^{-4}$	$3.09 \times 10^{-4}$	$2.97 \times 10^{-4}$
$\sigma_{\alpha_p}$ , m	$0.76 \times 10^{-4}$	$0.66 \times 10^{-4}$	$0.67 \times 10^{-4}$	$0.45 \times 10^{-4}$	$0.06 \times 10^{-4}$
$\eta_{es}$ , dimensionless	0.312	0.323	0.305	0.315	0.303

<sup>a</sup>Bromide ion tracer (grain diameter of 0.4–0.6);  $\alpha_c = 7.94 \times 10^{-4}$  m,  $D_m = 1 \times 10^{-9}$  m (fixed for all experiments.)

the bromide experiments were smoother than those from the fluorescein experiments.

## 6. Experiments Using a Cochlea

### 6.1. Device and Procedure

[30] The cochlear cavity was manufactured at Applied Process Equipment, Redwood City, CA and assembled at the Environmental Fluid Mechanics Laboratory at Stanford University. The cochlea was made of transparent polycarbonate (lexen), facilitating visual observation of the experiments. The inner ( $r_{in}$ ) and outer ( $r_{out}$ ) radii of the flow channel cavity at the inlet are 4.0 and 5.6 cm, respectively. The depth of the cochlear channel  $h_v$  in the vertical dimension is 2 cm and is kept uniform throughout the spiral. The cochlea has  $n = 3$  rotations with a radius increase factor  $\lambda$  of 1.6. A 3 mm thick mixing chamber was constructed at the inlet and outlet boundaries of the cochlea, which were constructed to be equipotentials of the analytical flow field. The mixing chambers allow the tracer to enter and leave the cochlear cavity through the entire cross section. The cochlear flow channel is formed after a PVC cap is screwed on top of the cochlear cavity. For preventing transverse leaking between the cochlea rotations, a layer of polyethylene closed cell adhesive foam tape was applied

between the cochlear cavity and the cap. On top of the foam, a water resistant and highly adhesive silicone compound was used for complete sealing.

[31] Packing was performed by introducing the glass beads in the cochlear cavity, closing the cap and applying pressure with high flow rate water injection. Then the cap was removed, and formed gaps would be filled with additional glass beads. The process was repeated until no apparent gaps were present. For comparison purposes, the same types of glass beads were used as in the helix. The cochlea was flushed with gaseous carbon dioxide prior to imbibition with degassed water to prevent gas entrapment. A constant flow rate was applied by a micropump provided by Ismatec, Switzerland. Breakthrough curves of tracer concentration were measured in the flow-through cell at the outlet of the device with the ion-selective electrode. Figure 4 shows a photograph of the cochlea in operation.

### 6.2. Experiments

[32] We performed two sets of bromide tracer experiments with a maximum concentration of 40 mg/L using different grain diameters in each set. The first set involved three tracer experiments at different flow rates. The cochlea was packed with glass beads ranging in diameter from 1.8 to 2.2 mm. The second set involved four tracer experiments

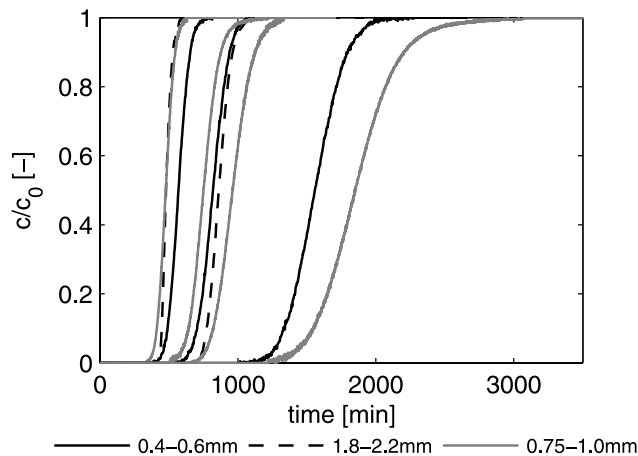


**Figure 3.** Normalized concentration breakthrough curves obtained in the helix experiments.

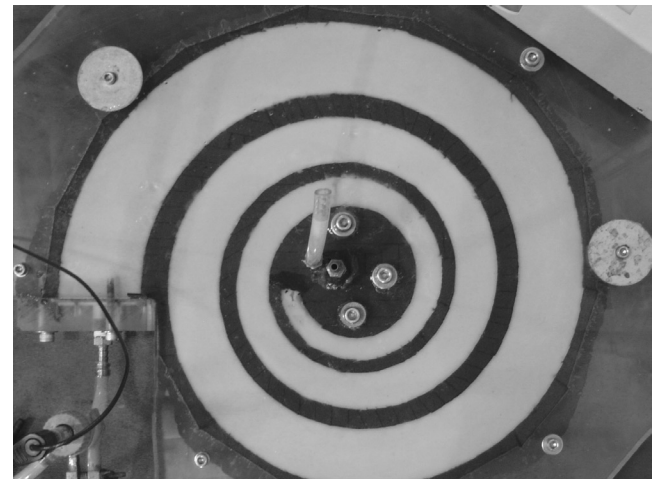


**Figure 4.** Plan view of the cochlea.

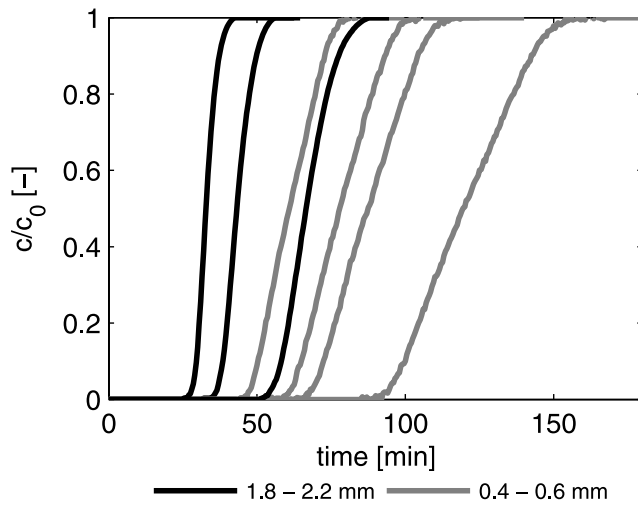


**Figure 5.** Normalized concentration breakthrough curves obtained in the cochlea experiments.

with glass beads ranging in diameter from 0.4 mm to 0.6 mm. The duration of the experiments ranged from one hour to four hours. The flow rates for these experiments are given in Tables 2 and 3. The breakthrough concentrations were measured in the flow-through cell and normalized by the inflow concentration. The normalized concentration breakthrough curves are shown in Figure 5. Similar to the tracer experiments in the helix,  $D_m$  contributed marginally to the transverse mixing because of the high flow rates applied. In addition to these experiments, we performed column experiments for determining the longitudinal dispersivity of the glass beads used in the filling. We obtained a longitudinal dispersivity  $\alpha_\ell = 0.0029$  m for the 1.8–2.2 mm packing and  $\alpha_\ell = 0.000794$  m for the 0.4–0.6 mm packing based on the fitting of the breakthrough curve to the analytical solution of *Ogata and Banks* [1962].

## 7. Numerical Simulations

### 7.1. Numerical Methods

[33] We simulated conservative transport in the helix and the cochlea by tracking 5000 particles in each model run. There exists no analytical solution for the flow field in the helix with finite pitch. We simulated the flow field within a cross section of the helix using the finite element method (FEM) with bilinear elements, assuming that the hydraulic gradient along the angular helical direction is constant. This flow field was compared to a full three-dimensional FEM simulation using trilinear elements, where the entire helix was modeled. The velocities obtained from these two models agreed, so that we continued with the computationally less expensive two-dimensional simulations in the following. We validated the particle-tracking method by simulating the case with a negligible pitch, for which *Cirpka and Kitanidis* [2001] had derived an analytical expression. The model passed this test.

[34] In the cochlea, the flow field is given by equations (12) and (13). The advective motion of particles in the cochlea is performed along predetermined streamlines. We validated the particle-tracking method by comparing concentration breakthrough curves obtained for strictly advective

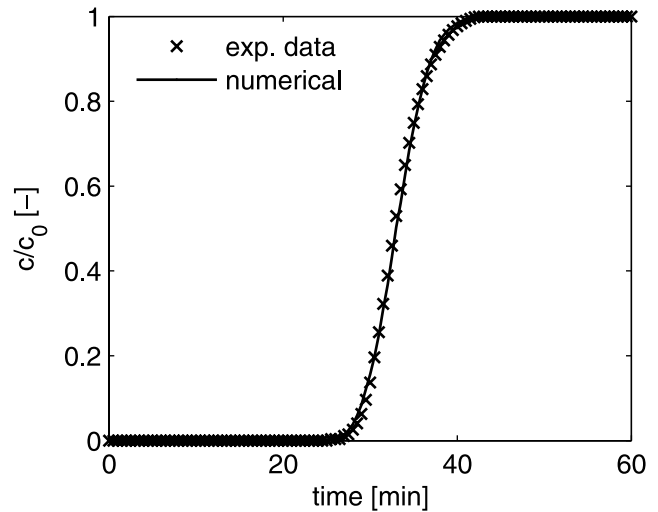


**Figure 6.** Experimental and simulated breakthrough curves for cochlea experiment 3, diameter of glass beads of 1.8–2.2 mm.

transport to results of an independent model based on the Matlab function *stream2* [*Luo and Kitanidis*, 2004]. The two simulated breakthrough curves matched.

[35] We estimated the parameters  $\alpha_t$  and  $\eta_e$  for single experiments by fitting the simulated breakthrough curve to the experimental one. Optimization was performed by the Levenberg-Marquardt method [*Press et al.*, 1992, section 15.5]. We tested the optimization procedure using a synthetic breakthrough curve with “true” values of  $\eta_e$  and  $\alpha_t$ . Subsequently, we estimated these parameters using arbitrary initial guesses. The optimization process returned the true values with an accuracy of 2%.

### 7.2. Results of Parameter Fitting and Sensitivity Analysis

[36] We estimated the parameters  $\alpha_t$  and  $\eta_e$  for each experiment independently. The effective diffusion coefficient  $D_m$  was fixed to  $1 \times 10^{-9}$  m<sup>2</sup>/s which is a rather

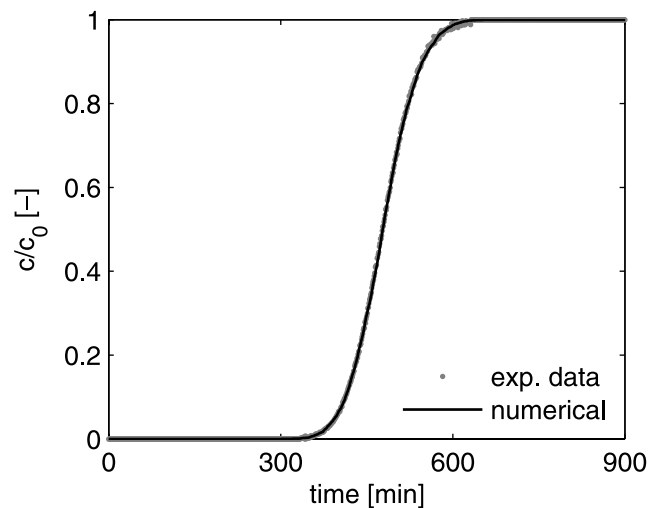


**Figure 7.** Experimental and simulated breakthrough curves for helix experiment 1, diameter of glass beads of 0.75–1.0 mm.

**Table 4.** Comparison of the Average Transverse Dispersivity and Standard Deviation Estimates for the Helix and Cochlea

	1.8–2.2 mm		0.4–0.6 mm	
	Helix	Cochlea	Helix	Cochlea
$\alpha_t, \times 10^{-3}$ m	1.25	1.19	0.276	0.297
95% $\alpha_t, \times 10^{-3}$ m	1.15–1.35	0.90–1.48	0.247–0.305	0.285–0.309

typical value for small molecules and ions in water at room temperature. The longitudinal dispersivity  $\alpha_L$ , determined from additional column experiments, and was kept constant in the optimization process.  $\alpha_L$  had a negligible contribution to the spreading of the concentration breakthrough curve in the helix experiments. On the contrary,  $\alpha_L$  contributed significantly to the breakthrough curve in the cochlea experiments. Tables 1, 2, and 3 list the flow rates, the estimated parameters, and their standard deviations for all tracer experiments. Figures 6 and 7 show the measured and fitted breakthrough curves for a cochlea and a helix experiment, respectively.

[37] The estimates of  $\eta_e$  were consistent for all sets of experiments and agreed satisfactorily with the rough estimate we obtained during the packing of the devices. Using the same glass beads, we obtained lower estimates of  $\eta_e$  in the cochlea than in the helix. This may be caused by more compact packing. In the cochlea, compaction is applied by flushing the cochlea with flow under high pressure as opposed to the air pressure applied in the helix. Different packing methods performed in a laboratory column with the same grains returned values of porosity ranging between 0.31 and 0.36.

[38] We obtained consistent estimates of  $\alpha_t$  within each set of experiments. Only in the fluorescein experiment in the helix with the highest flow rate (experiment 1 in Table 1), the estimated value of  $\alpha_t$  was considerably higher than in the other experiments performed with lower velocities using

the same filling. This observation may be an artifact resulting from the narrow width of the breakthrough curve. The estimates of  $\alpha_t$  obtained from the cochlea experiments were consistent with those obtained from the helix using the same filling. The 95% confidence intervals of the estimated parameters overlap for each set of experiments and also when comparing the estimated values from the helix and cochlea experiments for the same type of fillings (see Tables 2, 3, and 4). Table 5 provides estimates of  $\alpha_t$  obtained in the literature for packings of different grain sizes. We notice that our results are more in agreement with high estimates of  $\alpha_t$  relative to the grain diameter reported in the literature. We estimated values of the ratio  $\alpha_t/\alpha_L$  between 1/3 and 1/2, which is higher than the roughly 1/10 values reported by *Grane and Gardner* [1961], *Harleman and Rumer* [1963], and *Robbins* [1989]. However, ratios of  $\alpha_t/\alpha_L$  between 1/3 and 1/2 have also been reported in the literature and our results seem to be more in agreement with the findings of *Oostrom et al.* [1992] and *Szecsody et al.* [1994], who found similar  $\alpha_t/\alpha_L$  ratios and high estimates of  $\alpha_t$  relative to the grain diameter. One possible explanation for the high  $\alpha_t/\alpha_L$  ratios is that we used relatively uniform spheres which may tend to give lower longitudinal dispersion coefficients.

[39] Finally, we performed a sensitivity analysis to evaluate the impact of the longitudinal dispersivity  $\alpha_L$ , the effective diffusion coefficient  $D_m$ , the depth of the cochlear cavity  $h_c$ , and the initial inner radius  $r_{in}^0$  on the estimated parameters  $\alpha_t$  and  $\eta_e$  for the cochlea. In our optimization procedure, these parameters were assumed known. In the sensitivity analysis, we varied each parameter by a small increment and repeated the optimization process. Table 6 shows the relative change in the estimates of  $\alpha_t$  and  $\eta_e$  due to the perturbation of the model parameters from their base values.

[40] The sensitivity analysis reveals that  $D_m$  had no impact on the estimation of  $\alpha_t$  and  $\eta_e$ . This was anticipated since the hydrodynamic part of the dispersion tensor is by

**Table 5.** Comparison of the Estimates of Transverse Dispersivity for Different Grain Sizes and Flow Velocities Reported in the Literature With the Results Obtained in Our Experiments

Reference	$ v $ , m/d	$d$ , m	$\alpha_t$ , m
<i>Grane and Gardner</i> [1961]	0.14–345.6	$2.5 \times 10^{-4}$	$0.1–5.7 \times 10^{-4}$
<i>Grane and Gardner</i> [1961]	0.69–86.4	$7.4 \times 10^{-5}$	$0.6–0.96 \times 10^{-5}$
<i>Grane and Gardner</i> [1961]	0.14–86.4	$0.15 \times 10^{-4}$	$0.17–4.8 \times 10^{-4}$
<i>Harleman and Rumer</i> [1963]	10.02–245.4	$9.6 \times 10^{-4}$	$0.23–0.79 \times 10^{-4}$
<i>Hassinger and van Rosenberg</i> [1968]	0.21–0.3	$2.2–2.5 \times 10^{-4}$	$0.47–1.4 \times 10^{-4}$
<i>Hassinger and van Rosenberg</i> [1968]	0.71–37.6	$5.0–5.9 \times 10^{-4}$	$0.76–1.25 \times 10^{-4}$
<i>Robbins</i> [1989]	6.53–6.86	$4.8 \times 10^{-4}$	$0.0–0.88 \times 10^{-5}$
<i>Oostrom et al.</i> [1992]	1.08	$5.0 \times 10^{-4}$	$3.0–4.0 \times 10^{-4}$
<i>Szecsody et al.</i> [1994]	3.02	$1.5 \times 10^{-4}$	$1.7–6.3 \times 10^{-4}$
<i>Szecsody et al.</i> [1994]	172.8	$6.0 \times 10^{-4}$	$0.1–0.4 \times 10^{-4}$
<i>Susset</i> [1998]	0.63–2.72	$2.0–4.0 \times 10^{-3}$	$1.7–3.4 \times 10^{-4}$
<i>Seagren et al.</i> [1999]	2–29.2	$2.0 \times 10^{-3}$	$0.24–0.94 \times 10^{-4}$
<i>Susset</i> [1998]	2.3–25.7	$2.0 \times 10^{-3}$	$0.24–1.2 \times 10^{-4}$
<i>Susset</i> [1998]	0.1–10.0	$2.0 \times 10^{-3}$	$0.11–10.0 \times 10^{-4}$
<i>Susset</i> [1998]	0.1–10.1	$2.0 \times 10^{-3}$	$0.28–6.3 \times 10^{-4}$
<i>Eberhardt and Grathwohl</i> [2002]	1.7–3.4	$0.1–3 \times 10^{-3}$	$0.4–1.0 \times 10^{-4}$
<i>Klenk and Grathwohl</i> [2002]	1.53–11.33	$0.3–2 \times 10^{-3}$	$2.5–6.5 \times 10^{-4}$
<i>Huang et al.</i> [2003]	0.95–14.44	$2.1–3.0 \times 10^{-4}$	$5 \times 10^{-4}$
Our study (helix)	12.16–69.78	$1.8–2.2 \times 10^{-3}$	$1.2–1.3 \times 10^{-3}$
Our study (helix)	0.81–70.30	$0.75–1.0 \times 10^{-3}$	$3.15–5.52 \times 10^{-4}$
Our study (helix)	6.75–59.05	$0.4–0.6 \times 10^{-3}$	$2.50–3.03 \times 10^{-4}$
Our study (cochlea)	16.85–184.3	$1.8–2.2 \times 10^{-3}$	$0.9–1.39 \times 10^{-3}$
Our study (cochlea)	12.55–142.7	$0.4–0.6 \times 10^{-3}$	$2.85–3.09 \times 10^{-3}$

**Table 6.** Sensitivity Analysis of the Estimated Parameters<sup>a</sup>

Parameter	$\alpha_\ell$	$D_m$	$h_v$	$r_m^0$
Change from base case	+50.00%	+100.00%	+10.00%	+4.29%
Effect on $\alpha_t$	-31.29%	-0.42%	-0.29%	+7.86%
Effect on $\eta_e$	+0.03%	$\pm 0.00\%$	-9.10%	-7.68%
Change from base case	-50.00%	+500.00%	-10.00%	-4.29%
Effect on $\alpha_t$	+21.50%	-0.75%	+0.27%	-12.36%
Effect on $\eta_e$	-0.10%	$\pm 0.00\%$	+9.21%	+8.59%

<sup>a</sup>The change in the estimated parameter value is depicted for a given change in the model parameter.

an order of magnitude larger than  $D_m$ . Changes in  $\alpha_\ell$  only affected the estimates of  $\alpha_t$ , since  $\alpha_\ell$  only affects the relative spread of the breakthrough curves. By contrast,  $h_v$  only affected the estimate of  $\eta_e$ , because both  $h_v$  and  $\eta_e$  scale inversely with the seepage velocity. Changes in the initial inner radius  $r_m^0$  affected both  $\alpha_t$  and  $\eta_e$ . The sensitivity analysis suggests that a careful design of the device and an accurate determination of  $\alpha_\ell$  are needed in order to minimize the errors in the parameter estimates. On the contrary, in the helix experiments  $\alpha_\ell$  had practically no effect on the  $\alpha_t$  estimates.

## 8. Concluding Remarks

[41] In this study, we have performed conservative tracer experiments using two different devices, a helix and a cochlea, to determine the transverse dispersivity of homogeneous isotropic porous media. Both devices create shear flow where flow at the inside is faster than at the outside wall of the spiraling channel filled with the porous material. The shear flow causes spreading of the breakthrough curve in the outflow of the domain. Local transverse dispersion diminishes the spreading, resulting in apparent macrodispersion coefficients which are inversely related to the transverse dispersivity of the medium. This phenomenon is known as Taylor-Aris dispersion. The inverse relationship between local transverse dispersivity and longitudinal macrodispersion makes the approach attractive for the determination of small transverse dispersivity values, where methods based on analyzing transverse concentration profiles have the highest difficulties.

[42] For the chosen geometries, the relationship between local transverse dispersivity  $\alpha_t$  and observed spreading in the breakthrough curve is not exactly inverse because of early time effects (in both the helix and the cochlea), the influence of local longitudinal dispersion (predominantly in the cochlea), and nontrivial three-dimensional flow (in the helix). Thus, rather than relying on analytical solutions for idealized late time behavior, as suggested by *Cirpka and Kitanidis* [2001], we simulate flow and transport by numerical methods and incorporate the numerical model into a Levenberg-Marquardt optimization scheme to estimate the values of transverse dispersivity  $\alpha_t$  and effective porosity  $\eta_e$  from the measured breakthrough curves. Thus we have developed a complete simulation framework to estimate  $\alpha_t$  from tracer tests in laboratory devices using numerical simulation and optimization.

[43] Useful conclusions of the study concern mainly the use of the two experimental devices and the comparison of the parameter estimates obtained with the different

approaches. The cochlea is easier to fabricate than the helix, but attention must be given to the design. The cochlea is transparent and allows therefore visual observation of the course of the experiment when a dye tracer is added. The flow field in the cochlea is two-dimensional and can be solved analytically. The disadvantage of the cochlea is that it is limited to a small number of rotations and that the macroscopic spreading is not as intensive as in the case of the helix. As a consequence, estimating the transverse dispersivity  $\alpha_t$  requires to accurately determine the local longitudinal dispersivity  $\alpha_\ell$  of the packing by performing complementary column experiments. A sensitivity analysis showed that errors in the determination of  $\alpha_\ell$  translate into errors in the  $\alpha_t$  estimates. The flow in the helix is much more complex than in the cochlea and can be solved only numerically. Packing the helix is also more complicated. An advantage of the helix is that Taylor-Aris dispersion is more pronounced because more rotations can be included and the flow velocity does not decrease with the number of rotations.

[44] Our approach is advantageous compared to other approaches proposed in the literature where the  $\alpha_t$  estimates can be greatly affected by small-scale heterogeneities or measurement accuracy. Estimates of  $\alpha_t$  for the same material but obtained using different measurements that differ by an order of magnitude have been reported in the literature [*Hassinger and van Rosenberg*, 1968; *Robbins*, 1989]. The estimates of  $\alpha_t$  obtained from experiments in the helix and the cochlea are consistent for the same size glass beads. This observation holds for all experiment sets. Our method is noninvasive so that it does not disturb the flow. The method requires only a simple breakthrough curve at the outlet of the device, which is easy to obtain. However, it should be noted that our method is not geared to serious heterogeneity. In that case, a single breakthrough curve at the outlet would not be sufficient to determine the local transverse dispersivity.

[45] In our experiments, we consider the effective diffusion coefficient  $D_m$  to be constant. In future work the impact of  $D_m$  at different flow rates needs to be examined. Experiments with lower flow rates, where the hydrodynamic part of the dispersion tensor is of the same order of magnitude as  $D_m$ , should allow a joint determination of both parameters. A multioptimization approach is needed in this case where the breakthrough concentration curves of several sets of experiments will be fit simultaneously. This approach should provide the “global” parameters and a confidence interval for these estimated parameters that best fit all the experimental breakthrough curves.

[46] **Acknowledgments.** This material is based upon work supported by the National Science Foundation under grant NSF/EAR 0001441-002 and by the U.S. Environmental Protection Agency-sponsored Western Region Hazardous Substance Research Center under agreement R-828772. This article has not been reviewed by the agencies, and no official endorsement should be inferred. Any opinions, findings, and conclusions or recommendations expressed in this material are those of the authors and do not necessarily reflect the views of NSF or EPA. Additional funding is provided by the Emmy-Noether program of the Deutsche Forschungsgemeinschaft under grant Ci 26/3-4. We appreciate Arifur Rahman’s contribution in performing tracer experiments in the helix at Universität Stuttgart.

## References

Aris, R. (1956), On the dispersion of a solute in a fluid flowing through a tube, *Proc. R. Soc., Ser. A*, 235, 67–77.

- Bates, D. M., and D. G. Watts (1988), *Nonlinear Regression Analysis and Its Applications*, John Wiley, Hoboken, N. J.
- Bello, M. S., and R. Rezzonico (1994), Use of Taylor-Aris dispersion for measurement of a solute diffusion coefficient in thin capillaries, *Science*, 266, 773–776.
- Blackwell, R. J. (1962), Laboratory study of microscopic dispersion phenomena, *Soc. Pet. Eng. J.*, 2, 1–8.
- Brenner, H., and D. A. Edwards (1993), *Macrotransport Processes*, Elsevier, New York.
- Chen, J.-S., C.-S. Chen, H.-S. Gau, and C.-W. Liu (1999), A two-well method to evaluate transverse dispersivity for tracer tests in a radially convergent flow field, *J. Hydrol.*, 223(3–4), 175–197.
- Chu, M., P. K. Kitanidis, and P. L. McCarty (2005), Modeling microbial reactions subject to transverse mixing in porous media: When can the rates of microbial reaction be assumed to be instantaneous?, *Water Resour. Res.*, 41, W06002, doi:10.1029/2004WR003495.
- Cirpka, O. A. (2002), Choice of dispersion coefficients in reactive transport calculations on smoothed fields, *J. Contam. Hydrol.*, 58(3–4), 261–282.
- Cirpka, O. A., and P. K. Kitanidis (2000), Characterization of mixing and dilution in heterogeneous aquifers by means of local temporal moments, *Water Resour. Res.*, 36(5), 1221–1236.
- Cirpka, O. A., and P. K. Kitanidis (2001), Theoretical basis for the measurement of local transverse dispersion in isotropic porous media, *Water Resour. Res.*, 37(2), 243–252.
- Cirpka, O. A., E. O. Frind, and R. Helmig (1999), Numerical simulation of biodegradation controlled by transverse mixing, *J. Contam. Hydrol.*, 40(2), 159–182.
- Cirpka, O. A., Å. Olsson, Q. Ju, M. A. Rahman, and P. Grathwohl (2006), Determination of transverse dispersion coefficients from reactive plume lengths, *Ground Water*, 44(2), 212–221.
- Dentz, M., H. Kinzelbach, S. Attinger, and W. Kinzelbach (2000), Temporal behavior of a solute cloud in a heterogeneous porous medium: 1. Point-like injection, *Water Resour. Res.*, 36(12), 3591–3604.
- Eberhardt, C., and P. Grathwohl (2002), Time scales of organic contaminant dissolution from complex source zones: Coal tar pools versus blobs, *J. Contam. Hydrol.*, 59(2), 45–66.
- Fiori, A., and G. Dagan (2000), Concentration fluctuations in aquifer transport: A rigorous first-order solution and applications, *J. Contam. Hydrol.*, 45(1–2), 139–163.
- Gelhar, L. W., and C. L. Axness (1983), Three-dimensional stochastic analysis of macrodispersion in aquifers, *Water Resour. Res.*, 19(1), 161–180.
- Grane, F. E., and G. H. F. Gardner (1961), Measurements of transverse dispersion in granular media, *J. Chem. Eng. Data*, 6(2), 283–287.
- Ham, P. A. S., R. J. Schotting, H. Prommer, and G. B. Davis (2004), Effects of hydrodynamic dispersion on plume lengths for instantaneous bimolecular reactions, *Adv. Water Resour.*, 27(8), 803–813.
- Harleman, D. R. F., and R. R. Rumer (1963), Longitudinal and lateral dispersion in an isotropic porous medium, *Fluid Mech.*, 16, 385–394.
- Hassinger, R. C., and D. U. van Rosenberg (1968), A mathematical and experimental examination of transverse dispersion coefficients, *Soc. Pet. Eng. J.*, 8, 195–204.
- Huang, W. E., S. E. Oswald, D. N. Lerner, C. C. Smith, and C. Zheng (2003), Dissolved oxygen imaging in a porous medium to investigate biodegradation in a plume with limited electron acceptor supply, *Environ. Sci. Technol.*, 37(9), 1905–1911.
- Jellali, S. (2000), Pollution d'aquifères poreux par les solvants chlorés, mécanismes de transport avec échanges entre phases: Experimentations sur site contrôle avec le trichloroéthylène, technical report, Inst. Franco-Allemand de Rech. sur l'Environ., Strasbourg, France.
- Kapoor, V., and L. W. Gelhar (1994), Transport in three-dimensionally heterogeneous aquifers: 1. Dynamics of concentration fluctuations, *Water Resour. Res.*, 30(6), 1775–1788.
- Kapoor, V., and P. K. Kitanidis (1998), Concentration fluctuations and dilution in aquifers, *Water Resour. Res.*, 34(5), 1181–1193.
- Kapoor, V., L. W. Gelhar, and F. Miralles-Wilhelm (1997), Bimolecular second-order reactions in spatially varying flows: Segregation induced scale-dependent transformation rates, *Water Resour. Res.*, 33(4), 527–536.
- Kitanidis, P. K. (1994), The concept of the dilution index, *Water Resour. Res.*, 30(7), 2011–2026.
- Klenk, I., and P. Grathwohl (2002), Transverse vertical dispersion in groundwater and the capillary fringe, *J. Contam. Hydrol.*, 58(1–2), 111–128.
- Liedl, R., A. J. Valocchi, P. Dietrich, and P. Grathwohl (2005), Finiteness of steady state plumes, *Water Resour. Res.*, 31, W12501, doi:10.1029/2005WR004000.
- Lolic, A., S. Nikolic-Mandic, and P. Polic (2001), Optimization and application of the gas-diffusion flow injection method for the determination of chloride, *J. Serbian Chem. Soc.*, 66(9), 637–646.
- Luo, J., and P. K. Kitanidis (2004), Fluid residence times within a recirculation zone created by an extraction-injection well pair, *J. Hydrol.*, 295(1–4), 149–162.
- Nielsen, J. M., G. F. Pinder, T. J. Kulp, and S. M. Angel (1991), Investigation of dispersion in porous media using fiber-optic technology, *Water Resour. Res.*, 27(10), 2743–2749.
- Nishigaki, M., T. Sudinka, Y. Sasaki, M. Inoue, and T. Moriwaki (1996), Laboratory determination of transverse and longitudinal dispersion coefficients in porous media, *J. Groundwater Hydrol.*, 38(1), 13–27.
- Ogata, A., and R. B. Banks (1962), A solution of the differential equation of longitudinal dispersion in porous media, *U.S. Geol. Surv. Prof. Pap.*, 411-A.
- Oostrom, M., J. Hayworth, J. Dane, and O. Güven (1992), Behavior of dense aqueous phase leachate plumes in homogeneous porous media, *Water Resour. Res.*, 28(8), 2123–2134.
- Oya, S., and A. J. Valocchi (1998), Transport and biodegradation of solutes in stratified aquifers under enhanced in-situ bioremediation conditions, *Water Resour. Res.*, 34(12), 3323–3334.
- Press, W., S. Teukolsky, W. Vetterling, and B. Flannery (1992), *Numerical Recipes in FORTRAN 77: The Art of Scientific Computation*, 2nd ed., Cambridge Univ. Press, New York.
- Prickett, T. A., T. G. Naymik, and G. Lonquist (1981), A “random walk” solute transport model for selected groundwater quality evaluations, *Bull. Ill. State Water*, 65.
- Robbins, G. A. (1989), Methods for determining transverse dispersion coefficients of porous media in laboratory column experiments, *Water Resour. Res.*, 25(6), 1249–1258.
- Scheidegger, A. E. (1961), General theory of dispersion in porous media, *J. Geophys. Res.*, 66(10), 3273–3278.
- Seagren, E., B. Rittmann, and A. Valocchi (1999), An experimental investigation of NAPL pool dissolution enhancement by flushing, *J. Contam. Hydrol.*, 37(1–2), 111–137.
- Strack, O. (1989), *Groundwater Mechanics*, Prentice-Hall, Upper Saddle River, N. J.
- Susset, B. (1998), Quantifizierung des stoffübergangs von leichtflüchtigen chlorierten kohlenwasserstoffen (LCKW) im kapillarsaum des grundwassers, technical report, Univ. Tübingen, Tübingen, Germany.
- Szeccsody, J. E., F. Brockman, B. Wood, G. Streile, and M. J. Truex (1994), Transport and biodegradation of quinoline in horizontally stratified porous media, *J. Contam. Hydrol.*, 15(4), 277–304.
- Taylor, G. I. (1953), Dispersion of soluble matter in solvent flowing slowly through a tube, *Proc. R. Soc., Ser. A*, 219, 186–203.
- Wang, H., N. Crampon, S. Huberson, and J. Garnier (1987), A linear graphical method for determining hydrodispersive characteristics in tracer experiments with instantaneous injection, *J. Hydrol.*, 95, 143–154.
- Zou, S., and A. Parr (1993), Estimation of dispersion parameters for two-dimensional plumes, *Ground Water*, 31(3), 389–392.
- Zou, S., and A. Parr (1994), Two-dimensional dispersivity estimation using tracer experiment data, *Ground Water*, 32(3), 367–373.

I. D. Benekos, ENVIRON International Corporation, 6001 Shellmound Street, Suite 700, Emeryville, CA 94608, USA. (ybenecos-contact@stanfordalumni.org)

O. A. Cirpka, Swiss Federal Institute of Aquatic Science and Technology, Überlandstrasse 133, CH-8600 Dübendorf, Switzerland. (olaf.cirpka@eawag.ch)

P. K. Kitanidis, Department of Civil and Environmental Engineering, Stanford University, Stanford, CA 94305-4020, USA. (peterk@stanford.edu)